

High- T_c Superconductivity in doped boron-carbon clathrates

Simone di Cataldo,^{1,2} Shadi Qulaghasi,¹ Giovanni B. Bachelet,¹ and Lilia Boeri^{1,*}

¹*Dipartimento di Fisica, Sapienza Università di Roma, 00185 Roma, Italy*

²*Institute of Theoretical and Computational Physics,*

Graz University of Technology, NAWI Graz, 8010 Graz, Austria

(Dated: October 12, 2021)

We report a high-throughput *ab-initio* study of the thermodynamic and superconducting properties of the recently synthesized XB_3C_3 clathrates. These compounds, in which boron and carbon form a sponge-like network of interconnected cages each enclosing a central X atom, are attractive candidates to achieve high- T_c conventional superconductivity at ambient pressure, due to the simultaneous presence of a stiff B–C covalent network and a tunable charge reservoir, provided by the guest atom. Ternary compounds like CaB_3C_3 , SrB_3C_3 and BaB_3C_3 are predicted to exhibit $T_c \lesssim 50K$ at moderate or ambient pressures, which may further increase up to $77 K$ if the original compounds are hole-doped by replacing the divalent alkaline earth with a monovalent alkali metal to form ordered XYB_6C_6 alloys.

I. INTRODUCTION

The *hydride rush* initiated by the report of a superconducting critical temperature (T_c) of 203 K in SH_3 ^{1,2} completely reshaped the landscape of research on superconductivity, delivering the first example of room-temperature superconductivity after more than one century since its discovery,³ and introducing a new paradigm for material prediction heavily relying on computational methods.^{4–10}

The focus of the field is gradually shifting from achieving ever larger T_c 's to finding new high- T_c materials which can operate at (or close to) ambient pressure. Migdal-Eliashberg theory for superconductivity suggests that, besides hydrides,^{11,12} obvious candidates for observing high- T_c superconductivity from conventional (electron-phonon, hereafter *e-ph*) interaction are light-element compounds. In particular, boron and/or carbon compounds combine large phonon frequencies and covalent bonds, the two most important ingredients underlying high- T_c (conventional) superconductivity.^{13–15} Several theoretical predictions of conceivable high- T_c borides and carbides date back to the early 2000's, but none of them has been experimentally verified;^{16–20} twenty years later, the problem is being revisited with modern *ab-initio* methods for structural prediction, which permit to address the thermodynamic stability of different structures across the phase diagram.^{21,22} Last year, Zhu et al.²³ reported the formation of a previously unknown boron-carbon phase, with chemical formula XB_3C_3 , which is a structural analogue of high- T_c sodalite clathrate hydrides, like LaH_{10} , YH_6 etc.^{24–29} The structure, shown in Fig. 1, consists of a bcc lattice of interconnected *truncated octahedral* boron-carbon cages, each enclosing a guest X atom.

The empty B–C cage is dynamically and thermodynamically unstable at ambient pressure; however, a few XB_3C_3 compounds can be stabilized under pressure and exhibit a variety of attractive physical properties, such as superhardness (La) and ferroelectricity (Sc).^{23,30–32}

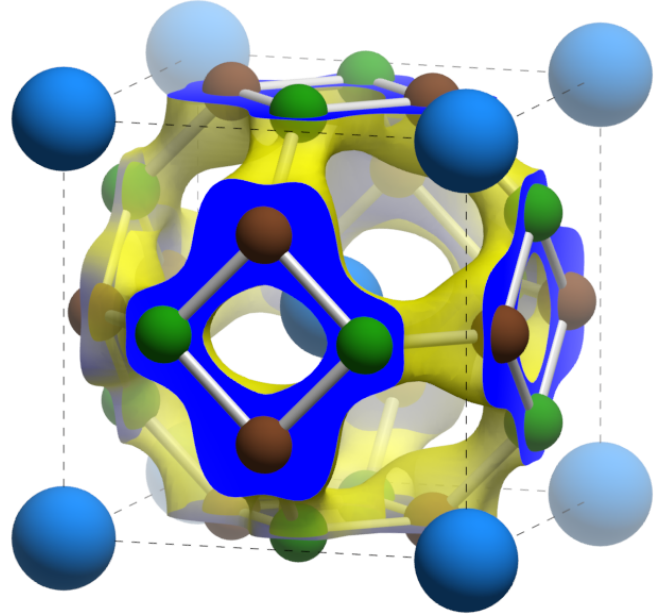


Figure 1. Crystal structure of XB_3C_3 . Space group: $Pm\bar{3}n$ (223); large blue, small brown and green spheres indicate X , B and C atoms, in Wyckoff positions $2a$, $6d$, and $6c$, respectively. The yellow isosurface, obtained for $X=Sr$ but representative of the valence-band-top wavefunction for all the XB_3C_3 compounds considered in this work (see also Fig.3), closely wraps the network of B–C bonds (see text); electric-blue lamellas mark its cross section at the cell boundaries.

SrB_3C_3 , which forms in diamond anvil cells at high pressure (57 GPa), but survives close to room pressure, has been theoretically predicted to superconduct below 40 K,³² a T_c close to the current record for ambient-pressure conventional superconductivity, held by magnesium diboride (MgB_2). Given the extreme versatility of cage-like structures observed in superhydrides, a suitable choice of the guest atom is likely to attain even higher T_c ; here we explore this possibility, by performing a detailed

study of thermodynamic and superconducting properties of hypothetical B-C clathrates, using first-principles methods based on Density Functional Theory (DFT).³³

Our sampling of conceivable compositions starts from an overall scan of the first 57 elements of the periodic table. We estimate the dynamical and thermodynamic stability of the XB_3C_3 compounds with $X = \text{H-La}$, and find that only five (Ca, Sr, Y, Ba, La) form stable XB_3C_3 compounds, none of which represents a substantial improvement over MgB_2 in terms of T_c and thermodynamic stability.

We then consider the possibility of combining pairs of the above elements to optimize the electronic properties in the direction of a higher T_c , and find a few ordered alloys XYB_6C_6 , where X and Y are mono- and di-valent elements, which should exhibit critical temperatures above the liquid nitrogen boiling point. These compounds form under pressure, but may be quenched down to room pressure without losing their remarkable properties; we argue that a further fine tuning of the doping level is very likely to give their T_c an extra boost.

II. COMPUTATIONAL DETAILS

Our calculations, based on the Density Functional Theory, were performed using Quantum ESPRESSO (QE),^{34,35} scalar-relativistic Optimized Norm-Conserving Vanderbilt pseudopotentials,³⁶ and a Perdew-Burke-Ernzerhof exchange-correlation functional.³⁷ The wavefunctions were expanded using a plane-wave basis set, with a cut-off of 80 Ry. The integration over the Brillouin zone was performed on a $6 \times 6 \times 6$ \vec{k} -space grid, using a Methfessel-Paxton³⁸ smearing width of 0.06 Ry. Such a choice ensures a 0.5 meV/atom convergence of the total energy and a 0.5 meV convergence of phonon frequencies.

The dynamical matrices and the related e - ph matrix elements were calculated using linear response theory.³⁹ The Brillouin zone was sampled on a $4 \times 4 \times 4$ \vec{q} -grid (phonons), and the integration of the e - ph matrix elements was carried out on a $30 \times 30 \times 30$ \vec{k} -grid (electrons) and a gaussian smearing width of 200 meV. The superconducting critical temperature was estimated by numerically solving the isotropic Éliashberg equations employing the Éliashberg functions obtained in linear response.

III. HIGH-THROUGHPUT STUDY OF XB_3C_3 CLATHRATE STABILITY

The main results of our initial high-throughput screening are summarized in Fig. 2.³³ For each of the first 57 elements of the periodic table ($X = \text{H-La}$), we performed a full relaxation of the XB_3C_3 structure at ambient pressure. For the relaxed structures, we computed the decomposition enthalpy with respect to the ground-state elemental structures $\Delta H = H(XB_3C_3) - (H(X) + 3H(B) + 3H(C))$, where $H(XB_3C_3)$ is the enthalpy of the XB_3C_3

structure relaxed at a given pressure, and $H(X)$, $H(B)$ and $H(C)$ are the enthalpies of the three elements in their ground-state structure at the same pressure.⁴⁰ This quantity is shown on a per/atom basis in Fig. 2; a comparison between $\Delta H(P = 0 \text{ GPa})$ and $\Delta H(P = 50 \text{ GPa})$ is shown in Fig. S2 of the Supplemental Material⁴¹.

Note that the decomposition enthalpy ΔH thus defined provides only a lower bound on the actual formation enthalpy. The latter also includes the decomposition into all possible binary and ternary phases on the hull, which is unfeasible in a high-throughput study. However, a negative $\Delta H(P)$ usually indicates that the phase will survive down to pressure P , if formed at higher pressure.

In our scan, only Ca, Y, and La are predicted to remain stable down to ambient pressure; and, indeed, LaB_3C_3 has been experimentally reported to form at 1 atm.³¹

The green-shaded region in Fig. 2 indicates the range of *metastability*, i.e. an energy region with $\Delta H > 0$, which encloses structures that may be synthesized under appropriate experimental conditions. Although there is no rigorous criterion for metastability, values of ΔH ranging from a few tens to a few hundreds meV are considered acceptable in literature;⁴² here we choose $\Delta H = 250$ meV, roughly corresponding to the average pV term at 50 GPa.

In addition to thermodynamic stability, Fig. 2 includes information on the *dynamical* (phonon) stability of XB_3C_3 compounds, estimated from linear-response calculations on a 2^3 grid in reciprocal space.³³ Compounds indicated with orange symbols have real (positive) frequencies on all points of the grid, while those with blue (empty) symbols have at least one negative (imaginary) optical frequency, and hence are dynamically unstable. Our criterion correctly classifies ferroelectric ScB_3C_3 as dynamically unstable.³⁰

A first inspection of the figure reveals that the formation of XB_3C_3 structures is energetically unfavorable for most elements in the periodic table; only three elements have negative formation enthalpies. Interestingly, all three compounds are predicted to be also *dynamically* stable, which is a strong indication that they may be synthesised, under appropriate conditions. In addition to the thermodynamically stable compounds at zero pressure, two more compounds, SrB_3C_3 and BaB_3C_3 , which have a positive decomposition enthalpy at ambient pressure, can be stabilized at higher pressure. The decomposition pressures (P_d), estimated by linear interpolation of the decomposition enthalpies between zero and 50 GPa, are 5 and 30 GPa in Sr and Ba, respectively. The corresponding formation pressures are expected to be significantly higher: for SrB_3C_3 , where experimental data exist, the difference is ~ 50 GPa. Assuming a similar shift, the formation pressure of BaB_3C_3 could be as high as 80 GPa.

The five elements which form stable XB_3C_3 compounds (i.e. Ca, Sr, Y, Ba, La) all belong either to the II A or to the III A group of the periodic table. An inspection of their electronic structure and of their structural data reveals that these elements lie in a sweet spot of valence and atomic radius; moreover, their low electroneg-

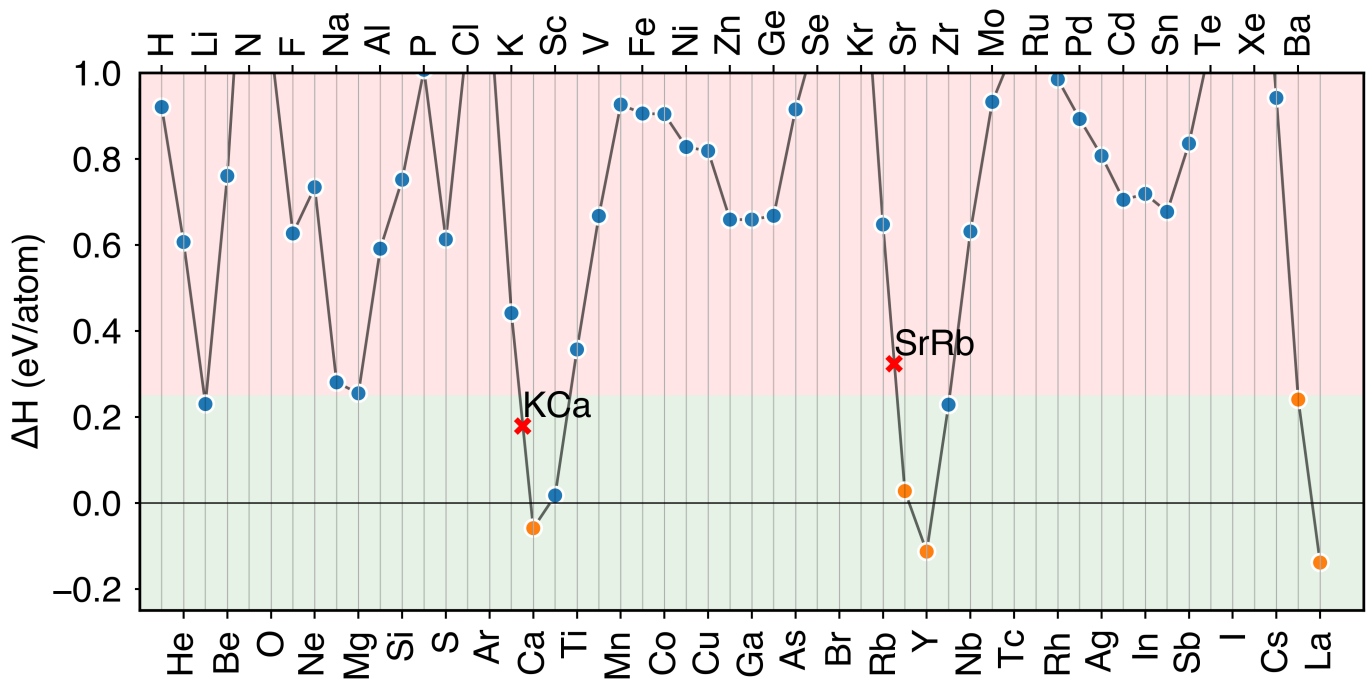


Figure 2. Decomposition enthalpy of XB_3C_3 compounds for the first 57 elements of the periodic table ($Z=1\dots 57$; the chemical symbol is shown above for odd- Z elements, below for even- Z elements). The color of markers relates to dynamical stability: blue dots indicate dynamically stable compounds, orange dots dynamically unstable. All quantities are calculated at $P=0$.

activity implies that, once within the B-C cage, they are completely ionized and their valence states do not mix with B-C states, and thus do not disrupt the stability of the structure. The dependence of the parameter on the X atom is shown in Fig. S1 of the Supplemental Material⁴¹.

IV. ELECTRONIC STRUCTURE

Fig. 3 shows an enlargement of the electronic structure in the Fermi level region for the five dynamically stable compounds at ambient pressure, and their immediate neighbors in the periodic table (K, Rb, Cs), arranged by period. For symmetry, we also include scandium, although dynamically unstable (ferroelectric³⁰). For each compound the energy zero is chosen in such a way as to coincide with the top of its valence bands; the position of its Fermi level is shown as a blue dashed line. Such a choice emphasizes the fact that the electronic bands of XB_3C_3 compounds with X belonging to the same period essentially follow a rigid-band model: in the valence region they are of almost pure B-C character; the guest X atoms, almost completely ionized, donate their charge to the B-C sublattice, filling its bands.

XB_3C_3 with the tri-valent guest elements Y and La are insulating: the 24 valence electrons are, in fact, sufficient to fill up the 12 B-C bonding bands, separated by a ~ 1 eV gap from the conduction bands, where antibonding B-C and X guest states do mix. Not so with

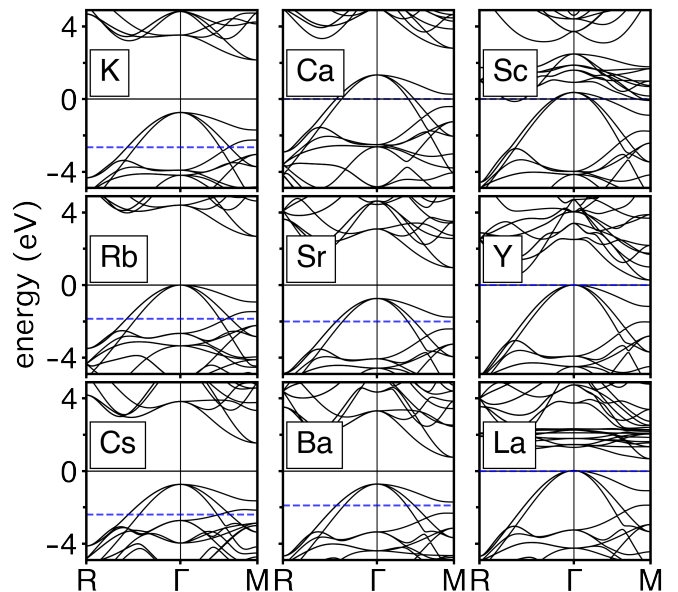


Figure 3. Band structure of the nine XB_3C_3 compounds considered in this work. The energy zero is set equal to the valence band tops, the Fermi energy is a blue dashed line.

Sc, whose d states, lower in energy, partially hybridize with the top of the valence band too, resulting in a poor metal (upper right panel of Fig.3).

Replacing tri- with di- and mono-valent elements (middle and left panels of Fig.3, respectively), the Fermi level

is shifted into the valence band, effectively doping it with holes. In Fig. 1 we show the XB_3C_3 crystal structure with an isocontour at one fourth of the maximum value of the squared modulus of the wavefunction at the top of the valence bands⁴³. The yellow iso-surface, obtained for $X=\text{Sr}$ but representative of the valence-band-top wavefunction for all the XB_3C_3 compounds appearing in Fig.3, closely wraps the network of B–C bonds. Holes doped into this band will experience an extremely strong e - ph coupling to bond-stretching phonons; a similar mechanism is at the heart of the remarkable superconducting properties of other B–C compounds, such as MgB_2 , boron-doped diamond, graphane.^{13,15,19,20,22,44} In XB_3C_3 , this very mechanism leads to substantial T_c 's. For metallic structures, using linear-response e - ph spectra and the McMillan-Allen-Dynes formula, assuming $\mu^* = 0.1$, we predict T_c values between 40 and 50 K – see table I. For Sr and Ca, calculations are performed at zero pressure, where the two compounds are dynamically stable; Ca has a very soft mode along the $\Gamma - M$ line. For Ba, which is dynamically unstable at ambient pressure, we report calculations at 30 GPa, where the compound is dynamically stable. In all cases, e - ph spectra are qualitatively very similar to those shown for the doped samples in Fig. 5 – See Figs. S3 to S8 of the Supplemental Material⁴¹; phonon frequencies extend up to ~ 100 meV; the e - ph coupling is spread over a wide range of frequencies, with a strong enhancement in the mid-frequency region where softer bond-stretching phonons are concentrated.

	P_d (GPa)	$\Delta H_{P=0}$ (meV/atom)	ω_{1og} (meV)	λ	T_c (K)
Ca	0	-91	17.5*	1.9	48
Sr	0	+5	51.0	1.0	44
Ba	30	+203	49.8	1.1	50

Table I. Calculated superconducting properties of stable XB_3C_3 compounds; the asterisk indicates that CaB_3C_3 experiences a remarked softening of one of the optical modes between M and Γ .

V. DOPING

The rigid-band behavior observed in Fig. 3 suggests that a partial substitution at the guest site may be used to improve the superconducting properties of alkaline-earth BC-clathrates. Fig. 4 shows an enlargement of the electronic Density of States (DOS) of SrB_3C_3 in the region around the Fermi level. It lies below the valence band top, within a $\sim 1\text{eV}$ -wide pseudogap which clearly separates a DOS shoulder, corresponding to a 1/2 hole/f.u. doping, from an equally tall sharp peak, corresponding to a 1/4 electron doping. While 1/4 electron doping requires a large supercell, 1/2 hole doping may be easily simulated by a simple cubic supercell, in which

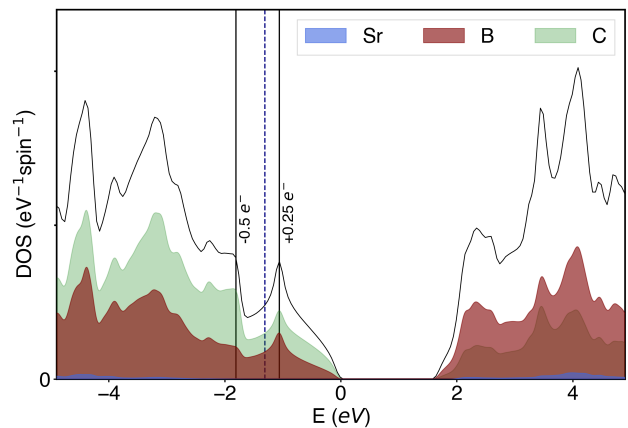


Figure 4. Electronic Density of States of SrB_3C_3 in the vicinity of the Fermi level (vertical dashed line). See text.

half of the divalent Sr atoms are replaced by monovalent Rb. At ambient pressure, such an ordered alloy is 12 meV/atom more stable than isolated SrB_3C_3 + isolated RbB_3C_3 , but its decomposition enthalpy with respect to the pure elements is high: $\Delta H=305$ meV/atom. In analogy to SrB_3C_3 , we expect that, at higher pressure, ΔH be reduced and SrRbB_6C_6 become stable. Following this line of reasoning, the estimated decomposition pressure would be $P_d = 42$ GPa.

For KCaB_6C_6 and CsBaB_6C_6 , obtained by doping CaB_3C_3 and BaB_3C_3 with K and Cs, respectively, the predicted decomposition pressures are 18 and 117 GPa – see table II. Hence, a correlation seems to emerge between the average atomic radius and the decomposition pressure: smaller atoms require lower pressure.

Fig. 5 shows the calculated phonon dispersions and Density of States of SrRbB_6C_6 , together with the e - ph Eliashberg spectral function $\alpha^2F(\omega)$. The corresponding figures for KCaB_6C_6 and CsBaB_6C_6 are shown in the Supplemental Material⁴¹. The e - ph coupling is mostly distributed on modes of the B–C host sublattice; a strong enhancement in the mid-frequency region, where soft bond-stretching phonons are concentrated, translates into a relatively low ω_{1og} (~ 44 meV) and a very large total e - ph coupling constant $\lambda=1.7$. Given the strong-coupling regime, we estimated the superconducting critical temperature by solving the full (isotropic) Migdal-Eliashberg equations. With a constant $\mu^* = 0.1$ we obtain a T_c of 77 K.

Table II reports the relevant superconducting parameters for the other two ordered alloys considered here. The quantities calculated at ambient pressure for KCaB_6C_6 are extremely close to those estimated for SrRbB_6C_6 . For CsBaB_6C_6 , which turns out to be weakly dynamically unstable at ambient pressure, we report results at 10 GPa; at this pressure, the predicted $T_c=82$ K is even slightly larger than the liquid nitrogen boiling point. These results indicate that, while the atomic radius has a major impact on pressure, its effect on T_c is almost negligible.

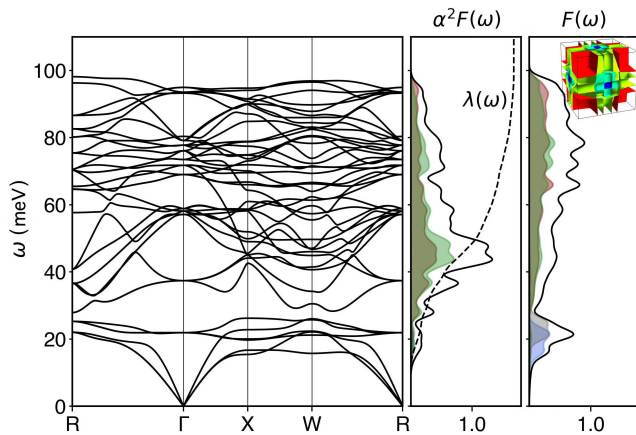


Figure 5. Phonon Dispersions (left), Density of States (middle), Eliashberg spectral function and Fermi surface (right) of SrRbB_6C_6 ($T_c = 77$ K).

	P ($\Delta H=0$) (GPa)	ΔH ($P=0$) (meV/atom)	ω_{\log} (meV)	λ	T_c (K)
KCa	18	+160	43.9	1.6	77
SrRb	42	+305	44.0	1.7	78
CsBa	117	+556	35.4*	2.2*	82*
B-diam ²²	–	+440	41.0	2.3	75

Table II. Predicted thermodynamic and superconducting properties of ordered alloys XYB_6C_6 ; quantities are defined as in table I. The asterisk reminds that for CsBa the superconducting parameters were calculated at $P=10$ GPa (see text). In the last row we report data for 50 % B-doped diamond, from Ref. 22. Note that, in that paper, T_c was estimated by the Mc-Millan-Allen-Dynes formula, while in the present work we employ the full solution of Migdal-Eliashberg equations, which is more accurate at strong coupling.

The data reported in table II suggest that doped XB_3C_3 compounds represent a substantial step forward in our understanding of conventional superconductors. Critical temperatures close to or larger than nitrogen boiling point (77 K) at room pressure have never been reported in any conventional superconductor so far; indeed, the current T_c record is much lower – 39 K in MgB_2 . On the last row of the table, we reported the corresponding data for heavily (50 %) B-doped diamond, which has also been predicted to exhibit T_c 's close to 80 K.^{19,22} It is remarkable to observe that the main superconducting parameters are extremely close, indicating similar lattice stiffness, bonding properties, nature and distribution of the e - ph coupling between diamond and XB_3C_3 structures. The key difference is that ΔH , in heavily B-doped diamond, is so high (~ 440 meV) that its experimental synthesis is likely impossible – the highest reported B-doping levels in diamond are 4-5 times smaller – while, according to our calculations, KCaB_3C_3 , similarly to SrB_3C_3 , could more easily form at moderate pressures, and then, once formed, it may be quenched down

to ambient pressure, without spoiling its substantial T_c . In addition, the empirical correlation between average atomic radii and stabilization pressure, the quasi-rigid-band behavior (Fig.3) and the steep energy dependence of the DOS at both edges of the pseudogap (Fig.4), suggest that both the synthesis conditions and the superconducting properties may be further improved by adjusting the doping level and/or combining atoms with different atomic radii.

VI. CONCLUSIONS

In conclusion, in this work we performed a broad-range study of the thermodynamic stability and superconducting properties of X -doped B–C clathrates XB_3C_3 . These compounds, recently synthesized under high pressure, are structurally related to record cage-like superhydrides like LaH_{10} and YH_6 , while their bonding and electronic properties, determined by the covalent B–C sublattice, are analogous to those of borides and carbides like MgB_2 ; and doped diamond.^{13,44}

Based on a full scan of the periodic table, we find that only five elements (Ca, Sr, Y, Ba and La) form stable XB_3C_3 compounds at ambient or moderate pressure. Two of them (La, Sr) have already been experimentally synthesized.^{23,31,32} While the superconducting T_c of ternary XB_3C_3 compounds are comparable to those of MgB_2 , the best conventional superconductor known so far, ordered alloys XYB_6C_6 containing mono- and divalent elements are, instead, expected to yield a substantial improvement, reaching T_c 's as high as 77 K. KCaB_6C_6 , where a high T_c ; coexists with a relatively moderate stabilization pressure (18 GPa), represents the most promising combination of elements among those considered here. A careful tuning of dopants and compositions may further increase T_c and/or reduce stabilization pressure.

Note: While writing this manuscript, we became aware of another study on superconductivity in doped XB_3C_3 compounds; its main results are in excellent agreement with ours.⁴⁵

ACKNOWLEDGMENTS

The authors acknowledge support from Fondo Ateneo-Sapienza 2017-2019. The computational resources were provided by CINECA through project IsC90-HTS-TECH_C, the Vienna Scientific Cluster (VSC) through Project P30269-N36 (Superhydra), and the dCluster of the Graz University of Technology. We thank Antonio Sanna for kindly sharing the code to numerically solve the isotropic Eliashberg equations

- * lilia.boeri@uniroma1.it
- ¹ A. P. Drozdov, M. E. M. I., I. Troyan, V. Ksenofontov, and S. Shylin, *Nature* **525**, 73 (2015).
 - ² D. Duan, Y. Liu, F. Tian, D. Li, X. Huang, Z. Zhao, H. Yu, B. Liu, W. Tian, and T. Cui, *Sci. Rep.* **4** (2014).
 - ³ E. Snider *et al.*, *Nature* **586**, 373 (2020).
 - ⁴ D. V. Semenov, I. A. Kruglov, A. G. Kvashnin, and A. R. Oganov, *arXiv preprint*, [arXiv:1806.00865](https://arxiv.org/abs/1806.00865) (2018).
 - ⁵ T. Bi, N. Zarifi, T. Terpstra, and E. Zurek, *arXiv preprint*, [arXiv:1806.00163](https://arxiv.org/abs/1806.00163) (2018).
 - ⁶ L. Boeri and G. B. Bachelet, *J. Phys. Condens. Matter* **31**, 234002 (2019).
 - ⁷ C. J. Pickard *et al.*, *Annu. Rev. Condens. Matter Phys.* **11**, 57 (2020).
 - ⁸ J. A. F. Livas *et al.*, *Phys. Rep.* (2020).
 - ⁹ A. Sanna *et al.*, *Phys. Rev. Lett.* **125**, 057001 (2020).
 - ¹⁰ L. Boeri, R. G. Hennig, P. J. Hirschfeld, G. Profeta, A. Sanna, E. Zurek, W. E. Pickett, M. Amsler, R. Dias, M. Eremets, C. Heil, R. Hemley, H. Liu, Y. Ma, C. Pierleoni, A. Kolmogorov, N. Rybin, D. Novoselov, V. I. Anisimov, A. R. Oganov, C. J. Pickard, T. Bi, R. Arita, I. Errea, C. Pellegrini, R. Requist, E. Gross, E. R. Margine, S. R. Xie, y. quan, a. hire, L. Fanfarillo, G. R. Stewart, J. J. Hamlin, V. Stanev, R. S. Gonnelli, E. Piatti, D. Romanin, D. Daghero, and R. Valenti, *Journal of Physics: Condensed Matter* (2021).
 - ¹¹ W. Chen, D. V. Semenov, X. Huang, H. Shu, X. Li, D. Duan, T. Cui, and A. R. Oganov, *Phys. Rev. Lett.* **127**, 117001 (2021).
 - ¹² S. Di Cataldo *et al.*, *Phys. Rev. B* **104**, L020511 (2021).
 - ¹³ J. Nagamatsu *et al.*, *Nature* **410**, 63 (2001).
 - ¹⁴ J. M. An and W. E. Pickett, *Phys. Rev. Lett.* **86**, 4366 (2001).
 - ¹⁵ L. Boeri, J. Kortus, and O. K. Andersen, *Phys. Rev. Lett.* **93**, 237002 (2004).
 - ¹⁶ H. Rosner *et al.*, *Phys. Rev. Lett.* **88**, 127001 (2002).
 - ¹⁷ M. Calandra, N. Vast, and F. Mauri, *Phys. Rev. B* **69**, 224505 (2004).
 - ¹⁸ A. N. Kolmogorov and S. Curtarolo, *Phys. Rev. B* **73**, 180501 (2006).
 - ¹⁹ J. E. Moussa *et al.*, *Phys. Rev. B* **77**, 064518 (2008).
 - ²⁰ G. Savini *et al.*, *Phys. Rev. Lett.* **105**, 037002 (2010).
 - ²¹ A. Jay *et al.*, *J. Appl. Phys.* **125**, 185902 (2019).
 - ²² S. Saha *et al.*, *Phys. Rev. B* **102**, 024519 (2020).
 - ²³ L. Zhu *et al.*, *Sci. Adv.* **6**, eaay8361 (2020).
 - ²⁴ A. P. Drozdov, V. Minkov, S. Besedin, P. Kong, M. Kuzovnikov, D. Knyazev, and M. Eremets, *arXiv preprint*, [arXiv:1808.07039](https://arxiv.org/abs/1808.07039) (2018).
 - ²⁵ Z. M. Geballe, H. Liu, A. K. Mishra, M. Ahart, M. Somayazulu, Y. Meng, M. Baldini, and R. J. Hemley, *Angewandte Chemie International Edition* **57**, 688 (2018).
 - ²⁶ A. Drozdov and et al., *arXiv preprint*, [arXiv:1812.01561](https://arxiv.org/abs/1812.01561) (2018).
 - ²⁷ H. Wang, J. S. Tse, K. Tanaka, T. Iitaka, and Y. Ma, *Proceedings of the National Academy of Sciences* **109**, 6463 (2012).
 - ²⁸ F. Peng, Y. Sun, C. J. Pickard, R. J. Needs, Q. Wu, and Y. Ma, *Phys. Rev. Lett.* **119**, 107001 (2017).
 - ²⁹ C. Heil *et al.*, *Phys. Rev. B* **99**, 220502 (2019).
 - ³⁰ L. Zhu, T. A. Strobel, and R. E. Cohen, *Phys. Rev. Lett.* **125**, 127601 (2020).
 - ³¹ T. A. Strobel, L. Zhu, P. A. Guńka, G. M. Borstad, and M. Guerette, *Angewandte Chemie International Edition* **60**, 2877 (2021), <https://onlinelibrary.wiley.com/doi/pdf/10.1002/anie.202012821>.
 - ³² J.-N. Wang, X.-W. Yan, and M. Gao, *Phys. Rev. B* **103**, 144515 (2021).
 - ³³ Computational Details can be found in sect. II.
 - ³⁴ P. Giannozzi, S. Baroni, N. Bonini, M. Calandra, R. Car, C. Cavazzoni, D. Ceresoli, G. L. Chiarotti, M. Cococcioni, I. Dabo, A. D. Corso, S. de Gironcoli, S. Fabris, G. Fratesi, R. Gebauer, U. Gerstmann, C. Gougoussis, A. Kokalj, M. Lazzeri, L. Martin-Samos, N. Marzari, F. Mauri, R. Mazzarello, S. Paolini, A. Pasquarello, L. Paulatto, C. Sbraccia, S. Scandolo, G. Sclauzero, A. P. Seitsonen, A. Smogunov, P. Umari, and R. M. Wentzcovitch, *Journal of Physics: Condensed Matter* **21**, 395502 (2009).
 - ³⁵ P. Giannozzi, O. Andreussi, T. Brumme, O. Bunau, M. B. Nardelli, M. Calandra, R. Car, C. Cavazzoni, D. Ceresoli, M. Cococcioni, N. Colonna, I. Carnimeo, A. D. Corso, S. de Gironcoli, P. Delugas, R. A. DiStasio, A. Ferretti, A. Floris, G. Fratesi, G. Fugallo, R. Gebauer, U. Gerstmann, F. Giustino, T. Gorni, J. Jia, M. Kawamura, H.-Y. Ko, A. Kokalj, E. Küçükbenli, M. Lazzeri, M. Marsili, N. Marzari, F. Mauri, N. L. Nguyen, H.-V. Nguyen, A. O. de-la Roza, L. Paulatto, S. Poncè, D. Rocca, R. Sabatini, B. Santra, M. Schlipf, A. P. Seitsonen, A. Smogunov, I. Timrov, T. Thonhauser, P. Umari, N. Vast, X. Wu, and S. Baroni, *J. Phys.: Condens. Matter* **29**, 465901 (2017).
 - ³⁶ D. R. Hamann, *Phys. Rev. B* **88**, 085117 (2017).
 - ³⁷ J. P. Perdew, K. Burke, and M. Ernzerhof, *Phys. Rev. Lett.* **77**, 3865 (1996).
 - ³⁸ M. Methfessel and A. T. Paxton, *Phys. Rev. B* **40**, 3616 (1989).
 - ³⁹ S. Baroni, S. de Gironcoli, A. Dal Corso, and P. Giannozzi, *Rev. Mod. Phys.* **73**, 515 (2001).
 - ⁴⁰ For all elements, we considered the ground-state structures under pressure, reported in literature; when the structures were not available, we employed structures predicted by evolutionary algorithm (USPEX).
 - ⁴¹ The Supplemental Material is available at *xxx*.
 - ⁴² M. Aykol, S. S. Dwaraknath, W. Sun, and K. A. Persson, *Science advances* **4**, eaq0148 (2018).
 - ⁴³ Specifically, since the dispersion relationship at the top of the valence band is threefold degenerate, we used the average of the squared modulus of the wavefunctions for the degenerate manifold.
 - ⁴⁴ E. A. Ekimov *et al.*, *Nature* **428**, 542 (2004).
 - ⁴⁵ P. Zhang, X. Li, X. Yang, H. Wang, H. Liu, and Y. Yao, *arXiv preprint*, [arXiv:2108.11026](https://arxiv.org/abs/2108.11026) (2021).